Journal of Materials Chemistry A

RSC Publishing

PAPER

View Article Online
View Journal | View Issue

Cite this: J. Mater. Chem. A, 2013, 1, 6433

Fabrication of well-arrayed plasmonic mesoporous TiO_2/Ag films for dye-sensitized solar cells by multiple-step nanoimprint lithography

Wei Jiang, Hongzhong Liu,* Lei Yin and Yucheng Ding

Received 1st March 2013
Accepted 28th March 2013

DOI: 10.1039/c3ta10882a

www.rsc.org/MaterialsA

This paper presents a photo-anode with well-arrayed plasmonic mesoporous TiO_2/Ag films for plasmon enhanced dye-sensitized solar cells. The patterned mesoporous TiO_2 nanostructure was implemented by multiple-step nanoimprint lithography (NIL), which can generate complex micro/nanostructures by successive imprinting on the same area using a combination of simpler flexible templates. Ag nanoparticles were introduced into the TiO_2 network by the photoreduction process to excite the plasmonic effect. Moreover, the morphological, material, optical and electrochemical properties of the patterned mesoporous TiO_2/Ag films were investigated by scanning electron microscopy, transmission electron microscopy, X-ray analysis, UV-Vis absorption spectroscopy and electrochemical impedance spectroscopy. The energy conversion efficiency and photocurrent density for patterned TiO_2/Ag cells were enhanced by about 24% and 25% as compared with those of the pure TiO_2 cells. The experimental observations demonstrate that the plasmonic effect can be enhanced by periodic patterns, allowing more broad light waves to couple to plasmonic wavelength due to the multiple reflection of incident light. The results also indicate that applying the multiple-step NIL process can not only increase the surface area of the photo-anode but also enhance the adherence at the TiO_2/TiO_2 nanoparticle interface and TiO_2/conductive substrate interface improving the electrochemical properties. With its simplicity and time-saving options, this method of fabricating patterned electrodes can be widely applied to a variety of large-area thin film solar cells.

1 Introduction

Dye-sensitized solar cells (DSSCs), an alternative to traditional photovoltaic devices due to their low cost and high efficiency,[1] have undergone considerable development in dye synthesis and device fabrication technologies. Recently the overall light to electricity conversion efficiency of DSSCs has reached as high as 12%, however, further improvement in the efficiency of DSSCs is still required for commercial and outdoor applications.

With absorption of light, the dye absorbed on the surface of TiO_2 particles can inject an electron into the TiO_2 network, where the injected electron travels through the network until collected. Simultaneously, the remaining dye radicals are reduced to a ground state by a redox-based mediator (typically I^-/I_3^-).[2] Generally, the efficiency of DSSCs is limited by the weak absorbance of the thin mesoporous TiO_2 film in the range of visible light. To solve this problem, increasing the mesoporous TiO_2 film thickness to a certain value has been proved to be useful for designing DSSCs. However, a much thicker TiO_2 film will go against the electrolyte diffusion, resist electrons flowing smoothly and aggravate charge recombination, which impose an upper limit on the film thickness.[3] These defects indicate that there is a trade-off between the light absorbance and the film thickness, leading to a compromised DSSC design and limiting the performance of DSSCs to some extent. To obtain a breakthrough, many methods have been extensively studied, such as adopting other nano-materials (ZnO (ref. 4 and 5) or TiO_2 (ref. 6 and 7) nanostructures, for instance), fabricating multicolored active layers,[8] substituting the platinized counter electrode,[9,10] or exploiting new dyes.[11–13] However, it is still difficult to simultaneously enhance the light absorption, carrier transport and charge collection. Therefore, determining how to make full use of the incident light, efficiently transfer electrons and reduce their recombination without affecting other factors is believed to be the key step in promoting the performance of DSSCs.

One promising approach to improve light absorption without increasing the photoactive layer thickness is to trap light in the active layer using an organized TiO_2 nanoparticle network. Arranging semiconductor materials in an orderly structure has become popular in the application of other photovoltaic devices since the patterned structure can form very unique light characteristics and has superior electrochemical properties.[14–16] Another potential strategy, surface plasmonic

State Key Laboratory for Manufacturing Systems Engineering, Xi'an Jiaotong University, Xi'an 710049, China. E-mail: hzliu@mail.xjtu.edu.cn; Fax: +86-29-83399508; Tel: +86-29-83399508

effect, has also been researched to increase the light absorption of the dye with minimal impact on other material properties, and application of the surface plasmonic effect to DSSCs has been investigated to obtain some exciting observations.[17–21] Nevertheless, most of the reports are based on planar structures and their studies are also mainly focused on the material properties, the structured plasmon enhanced DSSCs based on well-organized mesoporous TiO_2 films have been little reported.

To date, several studies have been performed to obtain patterned TiO_2 films for applications in optical waveguides, photocatalysis, and sensors, *via* template-assisted atomical layer deposition(ALD),[22] femtosecond laser pulses,[23] sol–gel precursor process,[24] electron beam lithography, and electro-hydrodynamic patterning. However, these studies focused on denser and thinner films, not suitable for DSSCs due to low dye absorption. Actually, the optimum active layer in DSSCs is the mesoporous TiO_2 film.[1] Until very recently, in comparison with the extensive studies on silicon solar cells and polymer solar cells, only a few approaches for patterning the mesoporous TiO_2 layer to trap light in the active layer have been reported. Grätzel and McGehee reported direct imprinting nanopatterning of TiO_2 paste with high pressure to produce disordered dome arrays by a quartz stamp, which is fragile, expensive and difficult to obtain in mass production.[25] Jeonghun Kim and Eunkyoung Kim also reported direct imprinting of well-arrayed nanopatterns of mesoporous TiO_2 films by PDMS stamp, which needs a long time and produces PDMS residues in the patterning process.[26]

Herein, to solve the above-mentioned problems, we present a multiple-step nanoimprint lithography (NIL) process using a Ni nanostamp to produce the complex well-organized TiO_2 films.[27] So far, most papers on NIL have reported on single-imprinting methods with thermoplastic and UV-curable resists, and also for which the same surface is imprinted only once and most of the produced patterns are simple 1D grating. However, the DSSCs would benefit from a versatile multiple-step NIL technique, where successive imprinting on the same area by the combination of simpler templates can generate complex structures, which can more effectively increase the optical path.[28] Compared to the conventional single imprinting technique, this is a very promising method for fabrication of patterned mesoporous TiO_2 films with different features, leading to a possibility of fabricating well-organized TiO_2 films on large-area substrates using a simple, speedy, and low-cost process in an atmospheric environment.

Below, direct multiple-step NIL on mesoporous TiO_2 films was performed to pattern mesoporous TiO_2/Ag films to achieve highly complex micro- and nano-scale architectures *via* a soft template based on a nickel nano-patterned mold, which has not been reported for the application of DSSCs and provides a new approach to fabrication and application of DSSCs. It allows for control of the grating profiles and has the capability of superimposing multiple patterns. Ag nanoparticles are introduced into the TiO_2 network by using a simple photoreduction method. The schematic diagram of the fabricated patterned TiO_2/Ag island array for plasmon-enhanced DSSCs is shown in Fig. 1, where the square island patterns are fabricated by NIL on the active layer combining the mesoporous TiO_2 film and Ag nanoparticles.

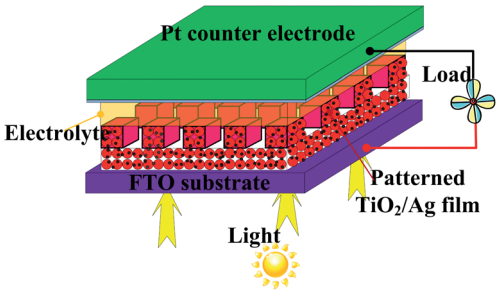

Fig. 1 Schematic diagram of DSSCs with the patterned mesoporous TiO_2/Ag film.

In this study, DSSCs based on planar TiO_2 films, planar TiO_2/Ag films and patterned TiO_2/Ag films have been fabricated, and the comparison among the three types of TiO_2 films is performed on aspects of morphology, light absorption, photovoltaic properties, and electrochemical characteristics. Furthermore, the light to electric energy conversion actually can be experimentally improved *via* patterns on the TiO_2/Ag film. This work is expected to provide a new approach for the fabrication and application of DSSCs.

2 Experimental

2.1 The preparation of patterned TiO_2/Ag photo-anodes

Porous TiO_2 films were fabricated by a doctor blading method onto the FTO glass plates with a viscous P25 based paste, which was prepared according to the reported literature.[29] All the homogeneous films were characterized by a 8 μm thickness transparent layer with the same active area 0.3 cm^2, which were measured using a surface profilometer. The nickel mold for NIL was replicated by electroforming from a template fabricated by laser interference lithography. The detailed procedures for the multiple-step NIL directly on TiO_2 films are shown in Fig. 2. Fig. 2(a)–(c) describe the first NIL which resembled single step imprinting and resulted in a set of line gratings. Firstly, the substrate was heated to 80 °C for 30 minutes to remove the partial solvents in the paste, leaving TiO_2 nanoparticles, ethyl cellulose and a small quantity of terpineol in the film. The following is the first NIL patterning process, which is imprinted with the temperature of the up and down pressure head at 70 °C under a pressure of 70 kg for 10 min using a commercial nanoimprinting machine. After the first NIL, the electrodes were sintered at 100 °C for 10 minutes to remove the terpineol completely, and Fig. 2(e)–(f) present the second NIL. Here we use the same stamp after a plane rotation of the stamp or sample by 90° *in situ*. The second NIL is preceded with the up and down pressure head at 110 °C under a pressure of 90 kg for 15 min. After all of the NIL processes, the TiO_2 film subsequently was sintered at 500 °C for half an hour to acquire a mesoporous TiO_2 film.

Subsequently, we would deposit Ag nanoparticles among the TiO_2 nanoparticles network. The mesoporous TiO_2 film was

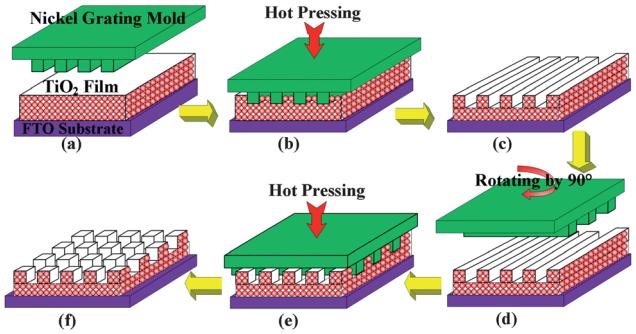

Fig. 2 Process flowcharts for the fabrication of a patterned mesoporous TiO_2 film by multiple-step NIL. (a) Stamp and sample preparation; (b) the stamp is applied on the TiO_2 film at 70 °C under a pressure of 70 kg for 10 min; (c) mold release and acquiring of the imprinted structures. (d) The same stamp is rotated by 90° in the local position. (e) The stamp is applied on the TiO_2 film at 110 °C under a pressure of 90 kg for 15 min; (f) mold release and results in complex structures after the multiple-step NIL.

immersed into a 3 mM $AgNO_3$ solution in absolute ethanol, which will allow Ag ions to more easily permeate into the TiO_2 particle network due to the polarity of ethanol, and also avoid the corrosion to Ag nanoparticles. Ten minutes later, the as-prepared films were washed several times with absolute ethanol to remove the excess Ag ions adsorbed on the surface. After drying under N_2 stream, the film was irradiated with UV light for 2 h to convert the Ag ions to Ag metal. Usually, the Ag islands are unstable in the I_3^-/I^- solution in DSSCs, in order to protect the Ag particles from corrosion, we also immersed the doped Ag photo-anodes into a tetrabutyl titanate solution for 30 min and then basted at 400 °C for 10 min.

2.2 DSSCs fabrication

Before dye adsorption, all the photo-anodes were treated with UV light and tetrabutyl titanate solution under the same conditions as used for the patterned TiO_2/Ag film. Then they were impregnated with a 0.3 mM N719 (dye Ruthenium 535-bisTBA, Solaronix, Switzerland, *cis*-diisothiocyanato-bis(2, 2-bipyridyl-4,4-dicarboxylatoe) ruthenium(II)bis (tetrabutylammonium)) absolute ethanol solution for 24 hours. The excess dye was removed from the electrode by rinsing with ethanol. As for the electrolyte solution, it was comprised of 0.6 M 1,2 dimethylimidazolium iodide (DMPII), 0.1 M LiI, 0.05 M I_2, 0.5 M *tert*-butylpyridine dissolved in acetonitrile. As for the counter electrode, a thin Pt layer was deposited on the conductive glass substrate by the rf-magnetron sputtering technique. An electrolyte-injecting hole was drilled on the counter electrode by ultrasound. The sandwich-type cell was fabricated by assembling the sensitized photo-anode with the counter electrode using hot pressing with a 60 μm thick Surlyn polymer film (Surlyn1702, Dupont). The electrolyte solution was injected into the drilled hole on the back side of the counter electrode and then drawn into the cell *via* the application of a vacuum. Finally, the punched hole was sealed with a 25 μm thick Surlyn polymer and a glass cover by hot pressing.

2.3 Characterization

The morphological properties of the TiO_2/Ag films were observed using a scanning electron microscope (SEM, CRESTEC CABL-9000C EBL, Japan) and a transmission electron microscope (TEM, JEOL JEM-2100F, Japan). The dimensions of the films were measured using a stylus profilometer (Ambios XP-2, USA). The crystalline phase compositions of the TiO_2 film were characterized using an X-ray diffractometer (XRD) using Cu Kα radiation, which was operated at 40 kV, 100 mA in the range 2θ from 20° to 80° and the scanning speed was 10° min^{-1} at a step of 0.04°. The chemical state of the Ag element in the photo-anode film was analyzed by X-ray photoelectron spectroscopy (XPS) using Mg Kα radiation. The UV-Vis absorption and reflection spectra were obtained with a JASCO-V570 UV-Vis-NIR spectrophotometer equipped with an integrating sphere accessory. The sandwich-type cells with the same active area 0.3 cm^2 were assembled to measure the photoelectrochemical properties of the dye sensitized solar cells. The photocurrent density–voltage (J–V) characteristics were measured using a 300 W xenon light source (calibrated with standard silicon based solar cells, AM 1.5G illumination, an intensity of 100 mW cm^{-2}) and a Keithley digital source meter (Model 2612). Electrochemical impedance was measured using a CHI-660D at a bias potential of the open circuit voltage (V_{oc}) and over the frequency range of 0.05–10^6 Hz with a 10 mV ac signal.

3 Results and discussion

3.1 The characterization of the patterned TiO_2/Ag photo-anode

3.1.1 The SEM morphology analysis. The SEM images of the patterned mesoporous TiO_2 films are shown in Fig. 3. Herein the direct multiple-step NIL on the TiO_2 active layer was implemented by a nickel grating mold with a period of 900 nm and depth of 280 nm. Fig. 3(a) shows the grating patterns after the first NIL, from which we can find that the direct NIL can be implemented in a large range, and the magnified image of Fig. 3(b) further shows that the porous TiO_2 grating can be imprinted to a depth of about 270 nm, very close to the depth of the template, which demonstrates that the flexible property of the nickel mold can ensure the conformal contact between the mold and the substrate, thus achieving a superior replication and reducing damnification to the mesoporous TiO_2 film.

Fig. 3(c) exhibits the TiO_2 ripples produced by incomplete secondary NIL for a short time. The magnified image, Fig. 3(d), displays the secondary TiO_2 ripples superimposed on the first NIL obtained TiO_2 gratings; the full structure of the nickel grating template was not replicated, which is affected by insufficient thermo-rheological properties of the ethyl cellulose based TiO_2 film due to insufficient time.

Fig. 3(e) presents the obtained TiO_2 square islands with complete secondary NIL for sufficient time, which demonstrates that the imprinting process can work well on a multiple-step patterning mesoporous TiO_2 film. Furthermore, the magnified image, Fig. 3(f), displays the full structure of the

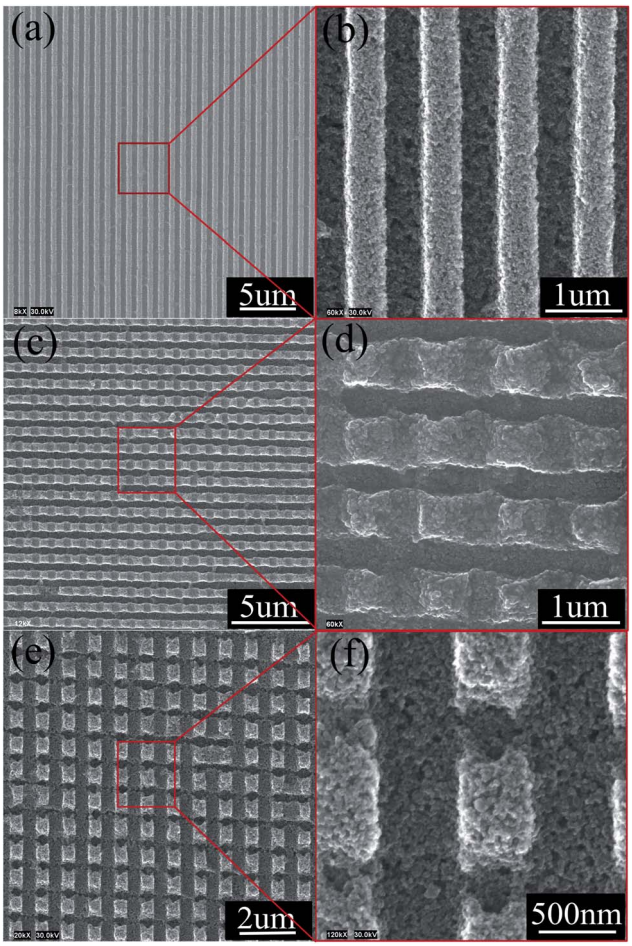

Fig. 3 The scanning electron microscopy pictures of patterns imprinted on the surface of mesoporous TiO_2 films. (a) Top view SEM image of TiO_2 gratings with submicron features by the first NIL; (b) the magnified SEM image of the grating characteristics. (c) TiO_2 ripples fabricated by the second NIL partially with the same nickel grating mold rotated by 90°; (d) the magnified SEM image of the TiO_2 ripple characteristics. (e) TiO_2 square islands fabricated by the second NIL completely with the same nickel grating mold rotated by 90°; (f) the magnified SEM image of the square island characteristics.

nickel grating template that was replicated on the surface of the TiO_2 grating pattern.

3.1.2 Ag element distribution and transmission electron microscopy (TEM) analysis. The Ag nanoparticles among the TiO_2/Ag network were not readily observed by the SEM images, but the Ag element distribution in depth can be confirmed by energy dispersive X-ray spectroscopy (EDS, AMETEK-EDAX Apollo-XL equipped Hitachi SU8010) with line scanning and elemental mapping analyses. As shown in Fig. 4, EDS line scanning data (Fig. 4(b)) of the cross-section indicate that the Ag element is distributed up to a deep position, and the EDS mapping data (Fig. 4(d)) show that the Ag element is distributed extensively throughout the whole film depth area. The TEM images of the synthesized TiO_2/Ag film are shown in Fig. 5(a), from which we can clearly find that Ag nanoparticles homogeneously attached on the surfaces of TiO_2 nanoparticles and no large aggregation of Ag nanoparticles is observed. Fig. 5(b) shows the high resolution TEM image of the synthesized TiO_2/Ag film,

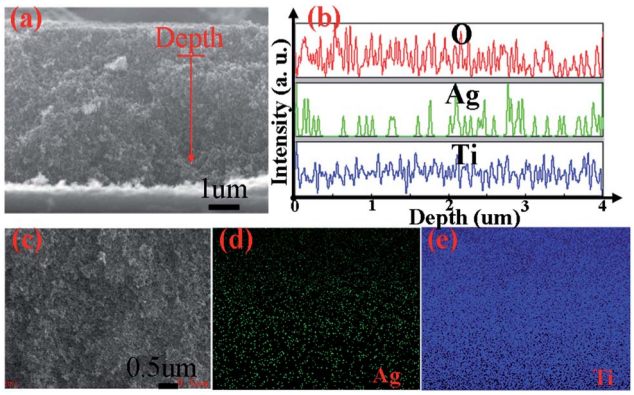

Fig. 4 (a) Cross-sectional SEM image for the deposited TiO_2/Ag film, (b) corresponding EDS element depth line scanning along the line shown in (a). (c) SEM cross-sectional views of the deposited mesoporous TiO_2/Ag film, (d) and (e) are the corresponding EDS mapping images for Ag and Ti elements with depth area.

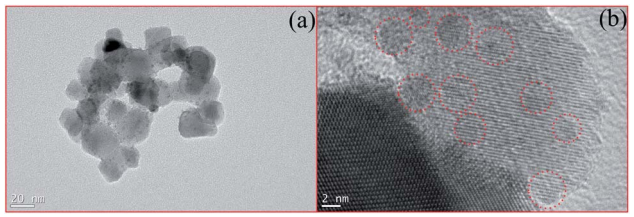

Fig. 5 (a) The transmission electron microscopy (TEM) image of the synthesized TiO_2/Ag film after UV exposure for 2 hours; (b) the high resolution TEM image of the crystalline structure of the TiO_2/Ag film.

which exhibited the lattice structure of TiO_2/Ag. The dotted circles represent the Ag nanoparticles, and we can find that the average particle size of the spherical Ag nanoparticles is about 5 nm in diameter. The existence of Ag nanoparticles is further confirmed by the following XRD and XPS measurements.

3.1.3 XRD and XPS analyses. Subsequently, the patterned TiO_2/Ag composite films were examined by XRD and XPS analyses to judge the presence of Ag nanoparticles and gauge the valence state of the Ag nanoparticles. Fig. 6 shows the XRD patterns of FTO glass (curve a), pure TiO_2 (P25) powders (curve b) and fresh TiO_2/Ag (curve c). It can be observed that after incorporation of Ag nanoparticles, the sample still showed usual anatase and rutile phases. Unexpectedly, no diffraction

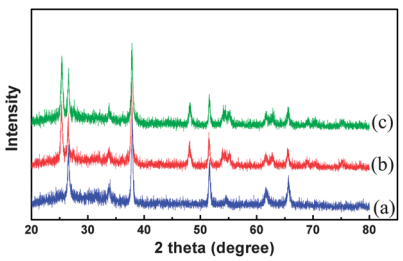

Fig. 6 X-ray diffraction (XRD) plots of FTO glass (curve a), TiO_2–FTO glass (curve b) and TiO_2/Ag–FTO glass (curve c) before impregnation of the dye.

peaks for Ag species (38.1, 44.2, 64.4, and 77.4°) were detected, which might be due to the low amount and the amorphous state of Ag. However, as shown in Fig. 7, the corresponding XPS spectra presented the detailed information of the obtained Ag nanoparticles. It shows that the Ag 3d spectra consisted of two individual peaks at ~374 and ~368 eV, which can be attributed to Ag 3d3/2 and Ag 3d5/2 binding energies, respectively. Moreover, the difference between the Ag 3d doublet is 6.0 eV, indicating the formation of metallic Ag nanoparticles.[30]

3.2 Optical properties of the patterned mesoporous TiO_2/Ag photo-anode

To investigate the optical properties of the patterned mesoporous TiO_2/Ag film, the UV-Vis absorption spectra of the various TiO_2 films were measured in the visible wavelength range (400–800 nm), which are shown in Fig. 8. It is known that under illumination, the Ag nanoparticles incorporated into the TiO_2 network can excite the surface plasmon resonance.[31,32] Compared to the pure unsensitized TiO_2 film the absorption spectrum of the unsensitized TiO_2/Ag film has a stronger red shifted peak at about 500 nm, which reveals that the introduced Ag nanoparticles can excite the plasmon resonance effect.[33] The dye-sensitized patterned TiO_2/Ag film and planar TiO_2/Ag film also present stronger absorption in the whole visible region compared to the sensitized pure TiO_2 film. It implies that the Ag nanoparticles can increase the light absorption of dye molecules due to the excited plasmonic effect under illumination.[34–36] Moreover, in comparison to the sensitized planar TiO_2/Ag film, the patterned sensitized TiO_2/Ag film also showed a much stronger light absorption. It demonstrated that the plasmonic effect was excited more effectively, broadly and deeply by applying the patterned structures, which can increase the optical path length by scattering or trapping the light, and allow more propagating light to couple to the surface of the active layer, thus plasmon resonance can be more efficiently excited on the surface of Ag nanoparticles to improve the light absorption of dyes.

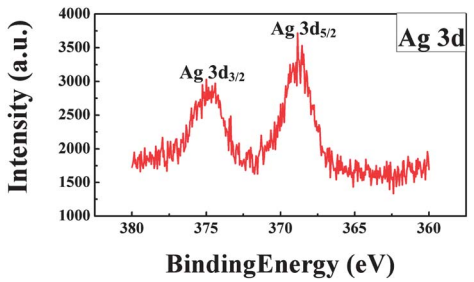

Fig. 7 X-ray photoelectron spectroscopy (XPS) spectrum of the TiO_2/Ag sample after UV irradiation.

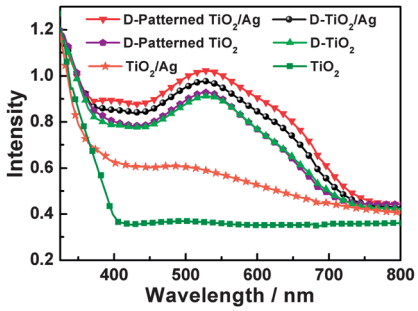

Fig. 8 UV-Vis absorption spectra of the photo-anodes by dye sensitized and unsensitized films.

3.3 Effect of the patterned mesoporous TiO_2/Ag film on the performance of DSSCs

According to the results of XRD, XPS and UV-Vis spectra measurements, the patterned TiO_2/Ag photo-anodes are expected to show excellent photovoltaic performance. To investigate the effect of the patterned mesoporous TiO_2/Ag film on the device performance, we studied the photovoltaic properties of the DSSCs based on the pure TiO_2 film, planar TiO_2/Ag film and patterned TiO_2/Ag film. In order to keep the effectiveness of the control measurements, the pure TiO_2 film was also treated with the UV light and tetrabutyl titanate solution under the same conditions as used for the planar TiO_2/Ag film and patterned TiO_2/Ag film.

Fig. 9(a) shows photocurrent density–voltage (J–V) characteristic curves from 0 V to 0.8 V in the dark. It clearly showed that the dark current of the DSSCs based on the TiO_2/Ag and patterned TiO_2/Ag photo-anodes decreased markedly than that for the pure TiO_2 film. The increase of the onset potential and the reduction of the dark current demonstrated that the introduced suitable Ag nanoparticles successfully reduced the recombination for the reduction of I_3^-. Moreover, the comparison of the DSSCs based on TiO_2/Ag and patterned TiO_2/Ag photo-anodes reveals that the introduced patterns also have some positive effects on suppressing the back reaction and enhancing the open voltage.

Fig. 9(b) shows the experimental photocurrent density–voltage (J–V) characteristics at AM 1.5 illumination of 100 mW cm^{-2}. The details are listed in Table 1. For the pure TiO_2, the open circuit photovoltage (V_{oc}) and short circuit current (J_{sc}) are 0.667 V and 10.04 mA, for TiO_2/Ag, they are 0.703 V and 11.04 mA, while for the as-prepared patterned TiO_2/Ag, they are 0.714 V and 12.70 mA. The generated conversion efficiency corresponds to 4.59%, 5.35% and 5.69% respectively. The above data show that silver containing cells are superior to silver-free cells

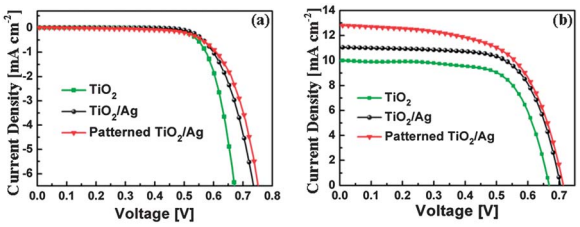

Fig. 9 (a) Dark current of the DSSCs based on pure TiO_2, planar TiO_2/Ag, and patterned TiO_2/Ag photo-anodes. (b) Photocurrent density–voltage characteristics of the DSSCs based on pure TiO_2, planar TiO_2/Ag, and patterned TiO_2/Ag photo-anodes.

Table 1 Comparison of characteristics for the DSSCs fabricated based on the pure TiO_2, TiO_2/Ag and patterned TiO_2/Ag photo-anodes

Samples	TiO_2	TiO_2/Ag	Patterned TiO_2/Ag
J_{sc} [mA cm^{-2}]	10.04	11.14	12.70
V_{oc} [V]	0.667	0.703	0.714
FF	0.687	0.683	0.627
η [%]	4.59	5.35	5.69
R_1 [Ω cm^2]	15.018	18.088	21.445
f [Hz]	19.95	15.85	12.59
Dye-loading [mol cm^{-2}]	5.32×10^{-18}	5.58×10^{-18}	5.61×10^{-18}

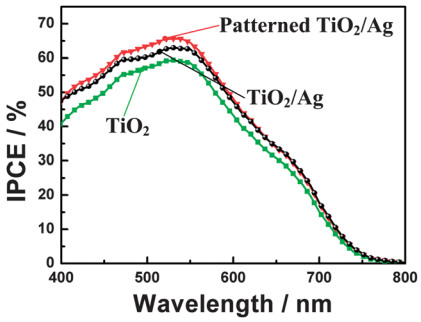

Fig. 10 The incident photon to current efficiency (IPCE) spectra of the DSSCs with the pure TiO_2, TiO_2/Ag and patterned TiO_2/Ag photo-anodes.

and the cells incorporated with the patterned mesoporous TiO_2/Ag film can further improve the photovoltaic performance.

The suppressive dark current for the introduced Ag nanoparticles indicates that the combination between Ag and TiO_2 nanoparticles may cause the conduction band edge of TiO_2 to shift negatively, increasing the gap between the Fermi level of the photo-anode and the redox potential under illumination, and as well Ag could act as active sites to inhibit the fast recombination of electron–hole pairs.[31,37] As for the patterned TiO_2/Ag film based solar cells, the decrease in dark current can be attributed to the enhanced adherence in the interface of TiO_2/TiO_2 and the interface of TiO_2–FTO substrate by the applied pressure in the NIL process, which decreases the recombination and resists the electron back reaction, resulting in the increase for the open circuit voltage.

As for the improved photovoltaic performance, on the one hand, the introduced nanoimprinted patterns make an optimum coupled electromagnetic field and improve the internal photoemission from the Ag nanoparticles, thus the increased Ag plasmonic effect enhances the optical absorption of the dye. On the other hand, the nanoimprinted patterns also increase the effective surface area at the TiO_2/dye/electrolyte, resulting in better charge collection. The above results are further verified by IPCE and EIS measurements as described in the following sections.

3.4 Incident photon-to-electron conversion efficiency measurement

To investigate the origin of the J_{SC} increase, we measured the incident photon-to-electron conversion efficiency (IPCE) spectrum. An IPCE measurement is more relevant than an UV-Vis absorption measurement to determine the enhancement in light harvesting efficiency for DSSCs. The IPCE is the yield of the number of electrons in the external circuit produced by an incident photon at a given wavelength, which can exclude the light absorption part that cannot effectively cause the light to electric conversion.[38–43]

Fig. 10 shows the IPCE spectra of the three studied DSSCs. It is found that the IPCE values increase in the order of the pure TiO_2 film, planar TiO_2/Ag film and patterned TiO_2/Ag film based solar cells. The planar TiO_2/Ag solar cells showed the enhancement in the almost whole visible region, which was consistent with the strong UV-Vis absorption spectrum. So the integrated Ag nanoparticles could promote light absorption throughout the visible region due to the excited plasmonic effect in the cell. Meanwhile, the IPCE spectrum of the DSSCs based patterned TiO_2/Ag by using the NIL technique showed a much larger increment. Considering the same photo-anode film thickness, such an increased IPCE increment in the visible region should primarily correspond to a much stronger light harvesting by integrated imprinted patterns. This enhancement was due to the increased optical path length within the patterned TiO_2/Ag thin film, resulting from multiple reflection of incident light. Thus, it demonstrated that the integrated patterns can improve the light absorption of the dyes more effectively to increase the photocurrent density.

3.5 Electrochemical impedance spectroscopy

To clarify the relationships between the performance of DSSCs and their internal resistances, we applied electrochemical impedance spectroscopy (EIS) measurements to analyze the results in the dark at a bias voltage of open circuit voltage V_{oc}. EIS measurements can effectively determine the interfacial charge transfer kinetics of DSSCs. In a typical EIS measurement, there are three semicircles in the Nyquist plot of DSSCs. The first semicircle in the high frequency range corresponds to the charge transfer reaction of I_3^-/I^- at the Pt/electrolyte interface; the second semicircle in the middle frequency range is mainly attributed to the charge transfer at the TiO_2/dye/electrolyte interface; the third semicircle stems from the diffusion of the electrolyte.[44,45]

Fig. 11 presents the EIS spectra, as the spacer is thin, so the information of the electrolyte diffusion is not obvious. Fig. 11(a) shows the typical equivalent circuit used to fit the EIS spectra.[46,47] Fig. 11(b) shows the Nyquist plots of EIS spectra and the resistances (R_1) corresponding to the second semicircles are listed in Table 1. The TiO_2/Ag based solar cells have a much larger R_1 value, in comparison to the pure TiO_2 based solar cells. This indicates that the doped Ag particles in TiO_2 films can reduce the recombination rate due to the better charge separation between the electrons and holes. Furthermore, among the three studied cells, the patterned TiO_2/Ag cell has the maximum R_1 value. This phenomenon is related to the introduced NIL technique, which improves the internal connection

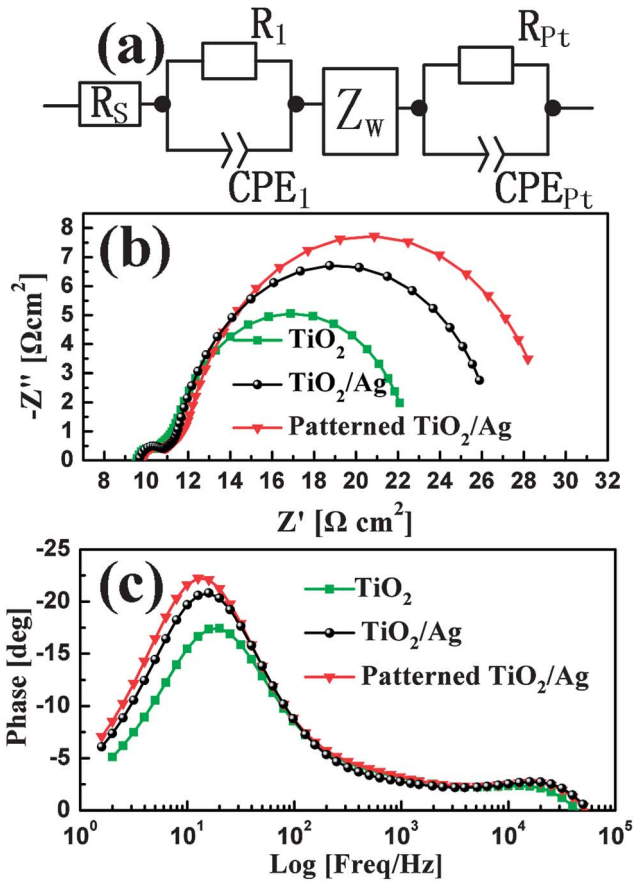

Fig. 11 (a) Equivalent circuit used to fit the EIS spectra for DSSCs: R_s is the series resistance; R_1 and CPE_1 represent the charge transfer resistance and the corresponding constant phase element at the TiO_2/dye/electrolyte interface; Z_w is the electrolyte diffusion resistance; R_{Pt} and CPE_{Pt} are the charge-transfer resistance and the corresponding constant phase element at the counter electrode; (b) Nyquist plots and (c) Bode phase plots for solar cells based on pure TiO_2, TiO_2/Ag, and patterned TiO_2/Ag photo-anodes.

of the TiO_2 nanoparticles and the adherence between the patterned TiO_2 film and the FTO substrate, thus the recombination on the interface of the TiO_2/electrolyte and the FTO/electrolyte is resisted to some extent. In the meantime, the patterned TiO_2/Ag based cells also provide a large contact surface area between the redox electrolyte and TiO_2 photo-anode, resulting in fast circular reactions. Therefore, the patterned TiO_2/Ag photo-anodes can effectively suppress the electron recombination, resulting favorably in a higher charge collection efficiency and photocurrent density, which is in good agreement with the photocurrent density–voltage characteristics and IPCE curves (shown in Fig. 9(b) and 10).

As mentioned above, the patterned TiO_2/Ag cell is expected to have a much longer lifetime and lower electron–hole recombination. As we know (according to the EIS model developed by Kern *et al.*), the relationship $\tau_e = 1/(2\pi f_{max})$,[48] which reveals the relationship between the electron lifetime (τ_e) and characteristic middle frequency. Fig. 11(c) shows the Bode phase plots of EIS spectra, which show the frequency peaks of the charge transfer process at different interfaces with the three studied cells, the detailed data are listed in Table 1. The f_{max} values of pure TiO_2, TiO_2/Ag, and patterned TiO_2/Ag are 19.95 Hz, 15.85 Hz, 12.59 Hz respectively, which reveals that the patterned TiO_2/Ag cell has the longest electron life time, and this is coincident with the Nyquist plots.

4 Conclusions

In summary, we have demonstrated that the multiple-step NIL of mesoporous TiO_2 films using flexible molds is a powerful method to build up complex structures from simpler templates. A periodical pattern with square island arrays for the mesoporous TiO_2 film was successfully fabricated on a transparent conductive substrate by soft thermal multiple-step NIL. The DSSCs assembled with patterned TiO_2/Ag photo-anodes were systematically investigated by optical and electrochemical measurements. The patterned TiO_2/Ag photo-anode proposed in this study apparently showed an enhancement in the short-circuit photocurrent and open-circuit photovoltage by 26.5% and 7.1%, compared to the reference cell with only a TiO_2 photo-anode. The improved performance is attributed to the further enhanced plasmonic effect due to the introduced periodical patterns, as well as to the superior electrochemical properties due to the increased interface adherence by the NIL technique. Therefore, the above method of fabricating complex structured photo-anodes by multiple-step NIL is also complementary to the development of photo-anode fabrication techniques for DSSCs. It is anticipated that the patterned TiO_2/Ag photo-anode design will provide an alternative approach to improve the performance of the DSSCs.

Acknowledgements

This work is supported by National Natural Science Foundation of China (no. 90923040, 51275400), National Science and Technology Project (no. 2011ZX04014-071), National Basic Research Program of China (no. 2009CB724202), and the Fundamental Research Funds for the Central Universities.

Notes and references

1 B. Oregan and M. Gratzel, *Nature*, 1991, **353**, 737–740.
2 C. Klein, E. Baranoff, M. K. Nazeeruddin and M. Gratzel, *Tetrahedron Lett.*, 2010, **51**, 6161–6165.
3 S. Ito, S. M. Zakeeruddin, R. Humphry-Baker, P. Liska, R. Charvet, P. Comte, M. K. Nazeeruddin, P. Péchy, M. Takata, H. Miura, S. Uchida and M. Grätzel, *Adv. Mater.*, 2006, **18**, 1202–1205.
4 Q. F. Zhang, C. S. Dandeneau, X. Y. Zhou and G. Z. Cao, *Adv. Mater.*, 2009, **21**, 4087–4108.
5 Y. Qiu, W. Chen and S. Yang, *J. Mater. Chem.*, 2010, **20**, 1001–1006.
6 J. H. Bang and P. V. Kamat, *Adv. Funct. Mater.*, 2010, **20**, 1970–1976.
7 J. Yan and F. Zhou, *J. Mater. Chem.*, 2011, **21**, 9406–9418.
8 K. Lee, S. W. Park, M. J. Ko, K. Kim and N.-G. Park, *Nat. Mater.*, 2009, **8**, 665–671.
9 J. Wu, Q. Li, L. Fan, Z. Lan, P. Li, J. Lin and S. Hao, *J. Power Sources*, 2008, **181**, 172–176.

10 J. Xia, L. Chen and S. Yanagida, *J. Mater. Chem.*, 2011, **21**, 4644–4649.
11 M. Grätzel, *Acc. Chem. Res.*, 2009, **42**, 1788–1798.
12 W. Wu, X. Xu, H. Yang, J. Hua, X. Zhang, L. Zhang, Y. Long and H. Tian, *J. Mater. Chem.*, 2011, **21**, 10666–10671.
13 P. Qin, X. Yang, R. Chen, L. Sun, T. Marinado, T. Edvinsson, G. Boschloo and A. Hagfeldt, *J. Phys. Chem. C*, 2007, **111**, 1853–1860.
14 A. Mihi, F. J. Lopez-Alcaraz and H. Miguez, *Appl. Phys. Lett.*, 2006, **88**, 193110.
15 Y. X. Gan, B. J. Gan, E. Clark, L. Su and L. Zhang, *Mater. Res. Bull.*, 2012, **47**, 2380–2388.
16 L.-Y. Lin, M.-H. Yeh, C.-P. Lee, Y.-H. Chen, R. Vittal and K.-C. Ho, *Electrochim. Acta*, 2011, **57**, 270–276.
17 A. Baba, K. Wakatsuki, K. Shinbo, K. Kato and F. Kaneko, *J. Mater. Chem.*, 2011, **21**, 16436–16441.
18 J. Qi, X. Dang, P. T. Hammond and A. M. Belcher, *ACS Nano*, 2011, **5**, 7108–7116.
19 B. Ding, B. J. Lee, M. Yang, H. S. Jung and J.-K. Lee, *Adv. Energy Mater.*, 2011, **1**, 415–421.
20 L. Bois, F. Chassagneux, C. d. Desroches, Y. Battie, N. Destouches, N. Gilon, S. p. Parola and O. Stéphan, *Langmuir*, 2010, **26**, 8729–8736.
21 X. Zhou, G. Liu, J. Yu and W. Fan, *J. Mater. Chem.*, 2012, **22**, 21337–21354.
22 X. D. Wang, E. Graugnard, J. S. King, Z. L. Wang and C. J. Summers, *Nano Lett.*, 2004, **4**, 2223–2226.
23 S. Passinger, M. S. M. Saifullah, C. Reinhardt, K. R. V. Subramanian, B. N. Chichkov and M. E. Welland, *Adv. Mater.*, 2007, **19**, 1218–1221.
24 M. J. Hampton, S. S. Williams, Z. Zhou, J. Nunes, D. H. Ko, J. L. Templeton, E. T. Samulski and J. M. DeSimone, *Adv. Mater.*, 2008, **20**, 2667–2673.
25 I. K. Ding, J. Zhu, W. Cai, S.-J. Moon, N. Cai, P. Wang, S. M. Zakeeruddin, M. Grätzel, M. L. Brongersma, Y. Cui and M. D. McGehee, *Adv. Energy Mater.*, 2011, **1**, 52–57.
26 J. Kim, J. K. Koh, B. Kim, J. H. Kim and E. Kim, *Angew. Chem.*, 2012, **124**, 6970–6975.
27 S. Y. Chou, P. R. Krauss and P. J. Renstrom, *J. Vac. Sci. Technol., B: Microelectron. Nanometer Struct.–Process., Meas., Phenom.*, 1996, **14**, 4129–4133.
28 C. Peroz, V. Chauveau, E. Barthel and E. Sondergard, *Adv. Mater.*, 2009, **21**, 555–558.
29 S. Ito, T. N. Murakami, P. Comte, P. Liska, C. Grätzel, M. K. Nazeeruddin and M. Grätzel, *Thin Solid Films*, 2008, **516**, 4613–4619.
30 H. Zhang, G. Wang, D. Chen, X. Lv and J. Li, *Chem. Mater.*, 2008, **20**, 6543–6549.
31 A. Takai and P. V. Kamat, *ACS Nano*, 2011, **5**, 7369–7376.
32 Y. Tang, P. Wee, Y. Lai, X. Wang, D. Gong, P. D. Kanhere, T.-T. Lim, Z. Dong and Z. Chen, *J. Phys. Chem. C*, 2012, **116**, 2772–2780.
33 K. Matsubara and T. Tatsuma, *Adv. Mater.*, 2007, **19**, 2802–2806.
34 C. Wen, K. Ishikawa, M. Kishima and K. Yamada, *Sol. Energy Mater. Sol. Cells*, 2000, **61**, 339–351.
35 Y. Hou, X. Li, Q. Zhao, X. Quan and G. Chen, *J. Mater. Chem.*, 2011, **21**, 18067–18076.
36 L. Yang, X. Jiang, W. Ruan, J. Yang, B. Zhao, W. Xu and J. R. Lombardi, *J. Phys. Chem. C*, 2009, **113**, 16226–16231.
37 K. D. Schierbaum, S. Fischer, M. C. Torquemada, J. L. de Segovia, E. Román and J. A. Martín-Gago, *Surf. Sci.*, 1996, **345**, 261–273.
38 C. H. Lee, S. W. Rhee and H. W. Choi, *Nanoscale Res. Lett.*, 2012, **7**, 48.
39 S. C. Choi, H. S. Lee and S. H. Sohn, *Adv. Powder Technol.*, 2012, **23**, 866–871.
40 L. Li, E. A. Gibson, P. Qin, G. Boschloo, M. Gorlov, A. Hagfeldt and L. Sun, *Adv. Mater.*, 2010, **22**, 1759–1762.
41 S. H. Kang, J.-Y. Kim, Y. Kim, H. S. Kim and Y.-E. Sung, *J. Phys. Chem. C*, 2007, **111**, 9614–9623.
42 X.-H. Zhang, Z.-S. Wang, Y. Cui, N. Koumura, A. Furube and K. Hara, *J. Phys. Chem. C*, 2009, **113**, 13409–13415.
43 Q.-H. Yao, F.-S. Meng, F.-Y. Li, H. Tian and C.-H. Huang, *J. Mater. Chem.*, 2003, **13**, 1048–1053.
44 M. Adachi, M. Sakamoto, J. Jiu, Y. Ogata and S. Isoda, *J. Phys. Chem. B*, 2006, **110**, 13872–13880.
45 Q. Wang, J.-E. Moser and M. Grätzel, *J. Phys. Chem. B*, 2005, **109**, 14945–14953.
46 M. Itagaki, K. Hoshino, Y. Nakano, I. Shitanda and K. Watanabe, *J. Power Sources*, 2010, **195**, 6905–6923.
47 Q. Wang, S. Ito, M. Grätzel, F. Fabregat-Santiago, I. Mora-Seró, J. Bisquert, T. Bessho and H. Imai, *J. Phys. Chem. B*, 2006, **110**, 25210–25221.
48 R. Kern, R. Sastrawan, J. Ferber, R. Stangl and J. Luther, *Electrochim. Acta*, 2002, **47**, 4213–4225.

